Multiscale understanding of surface structural effects on high-temperature operational resiliency of layered oxide cathodes

Xiang Liu, Xinwei Zhou, Qiang Liu, Jiecheng Diao, Chen Zhao, Luxi Li,* Yuzi Liu,* Wenqian Xu, Amine Daali, Ross Harder, Ian K. Robinson, Mouad Dahbi, Jones Alami, Guohua Chen, Gui-Liang Xu* and Khalil Amine*

Dr. X. Liu, Dr. C. Zhao, A. Daali, Dr. G.-L. Xu, Dr. K. Amine

Chemical Sciences and Engineering Division, Argonne National Laboratory, Lemont, IL 60439, USA

Email: xug@anl.gov and amine@anl.gov

Dr. X. Zhou, Dr. Y. Liu

Centre for Nanoscale Materials, Argonne National Laboratory, Lemont, IL 60439, USA

Email: yuziliu@anl.gov

Dr. Q. Liu, Prof. G. Chen

Department of Mechanical Engineering and Research Institute for Smart Energy (RISE), The Hong Kong Polytechnic University, Kowloon, Hong Kong, China

J. Diao, Prof. I. Robinson

London Centre for Nanotechnology, University College London, London WC1E 6BT, U.K.

Dr. L. Li, Dr. W. Xu, Dr. R. Harder

X-ray Science Division, Advanced Photon Source, Argonne National Laboratory, Lemont, IL 60439, USA, Email: luxili@anl.gov

Dr. Mouad DAHBI, Prof. Jones ALAMI

This article has been accepted for publication and undergone full peer review but has not been through the copyediting, typesetting, pagination and proofreading process, which may lead to differences between this version and the Version of Record. Please cite this article as doi: 10.1002/adma.202107326.

Materials Science and Nano-Engineering Department, Mohammed VI Polytechnic University, Ben Guerir, Morocco

Prof. I. Robinson

Condensed Matter Physics and Materials Science Department, Brookhaven National Laboratory, Upton, New York 11793, United States

Dr. K. Amine

Materials Science and Engineering, Stanford University, Stanford, CA 94305, USA

Dr. X. Liu, Dr. X. Zhou and Dr. Q. Liu contributed to this work equally.

Key words: High temperature; calendar aging; thermal runaway; surface structures; layered cathode

Abstract: The worldwide energy demand in electric vehicles and the increasing global temperature have called for development of high-energy and long-life lithium-ion batteries (LIBs) with improved high temperature operational resiliency. However, current attention has been mostly focused on cycling aging at elevated temperature, leaving considerable gaps of knowledge in the failure mechanism and practical control of abusive calendar aging and thermal runaway that are highly related to the eventual operational lifetime and safety performance of LIBs. Herein, using a combination of various *in situ* synchrotron X-ray and electron microscopy techniques, we report a multiscale understanding of surface structure effects involved in regulating the high temperature operational tolerance of polycrystalline Ni-rich layered cathodes. Our results collectively show that an ultraconformal poly (3,4-ethylenedioxythiophene) coating can effectively prevent $LiNi_{0.8}Co_{0.1}Mn_{0.1}O_2$ cathode from undesired phase transformation and transition metal dissolution on the surface, atomic displacement and dislocations within primary particles, intergranular cracking along the grain boundaries within

secondary particles, and intensive bulk oxygen release during high state-of-charge and high temperature aging. The present work highlights the essential role of surface structure controls in overcoming the multiscale degradation pathways of high-energy battery materials at extreme temperature.

1. Introduction

The invention and commercialization of lithium-ion batteries (LIBs) have brought an energy revolution and significantly boosted the electrification process of our world. With the exponentially increasing demand for energy storage, it is expected that LIBs need to allow for stable operation beyond room temperature.[1, 2] This comes from the fact of regional and seasonal temperature fluctuations as well as the increasing global temperature. In addition, some task-specific applications such as aerospace missions and medical devices are required to operate under extreme environments such as high temperature. However, previous studies have shown that high-capacity layered oxide cathodes such as $LiNi_xCo_yMn_{1-x-y}O_2$ (hereafter denoted as NCM) are susceptible to undesired structural transformation and particle cracking during charge/discharge at elevated temperature.[3] Moreover, when the temperatures soar, the commercial $LiPF_6$-based electrolytes tend to undergo a disproportionation reaction generating detrimental HF even in the presence of trace protic impurities, which can severely erode the NCM cathodes.[4] Furthermore, the aggravated parasitic reactions at the electrode-electrolyte interface during high temperature are known to deteriorate the cathodes' structures and thicken the interface layer, leading to dramatic increase of cell impedance during cycling.[5]

Calendar aging of LIBs while they are not used is another critical challenge to their real operational lifetime, but has been paid much less attention in comparison with cycling aging.[6] In general, LIBs are stored or shipped at high state-of-charge (SoC) to ensure their immediate use upon receipt (e.g. military batteries). Meanwhile, most of LIBs spend much of their lifetime to be used, which means that they will

be exposed to the working environments at certain SoC and temperature with long resting periods after intermittent use (e.g. electric vehicles). Ecker et al. have reported that the capacity fade and resistance of NCM/carbon 18650 LIBs increased along with elevated storage temperature and SoC due to the continuous growth of solid-electrolytes interphase (SEI) on the negative electrode during calendar aging test.[7] While Ryu et al. revealed that the performance degradation of Li/Ni-rich NCM cells during high-temperature storage originate from the exacerbated side reactions between electrolytes and charged NCM cathodes that contained highly active Ni^{4+}.[8] These undesired reactions resulted in the formation of NiO-like phase rock-salt structure with tens of nanometers on the surface of the primary particles and further microcracks along the grain boundaries. Hu et al. further pointed out that SoC play a more prominent effect in accelerating the decomposition of electrolytes over storage temperature.[9] At high SoC, even with exposure to a high temperature for only a short period, such thermal memory can significantly accelerate the self-discharge of LIBs using $LiCoO_2$ cathode.[10] Despite considerable efforts in the mechanistic understanding, mitigation of calendar aging and the underlying mechanism remain largely ignored, which however need to be paid more attention in particular for military, electric vehicles and large-scale stationary energy storage systems that will be exposed to various outdoor temperature conditions.

Thermal runaway of LIBs can lead to the generation of a huge amount of heat in a short period of time and further battery explosion, posing serious safety concern for their large-scale deployment.[11] Our previous study has revealed that the delithiated Ni-rich NCM cathodes would trigger a layered-to-spinel structure transformation and generation of huge amount of O_2 when exposed to high temperature.[12] We have also revealed that these charged cathodes released gases (e.g. O_2) will undergo chemical crosstalk from cathode to anode side, and further react with lithiated anode and electrolytes, resulting in the intensive exothermic reactions and significant increase of cell temperature to even over 800 ^{o}C.[13, 14] Although most LIBs will not work under such high temperature, the thermal tolerance of

cathodes at high temperature is indeed one of the critical factors for the high temperature operation resiliency of LIBs.

To date, various surface coating strategies have been attempted to improve the durability/longevity of layered oxide cathodes at high temperature.[15-17] However, the reported cycle stability at high-temperature remains far less satisfied.[16-20] Moreover, most of these coating approaches have not been carefully evaluated under more rigorous conditions such as high temperature and high SoC calendar aging, raising a serious question on the robustness of coating layers under harsh working environments. Meanwhile, the explicit role of surface coating in improving the thermal tolerance of layered cathodes remains elusive. Therefore, the design criteria of rational surface protection to effectively improve the high temperature operational resiliency of LIBs has not been well established yet.

In this work, we unraveled the role of ultra-conformal poly (3, 4-ethylenedioxythiophene) (PEDOT) coating in suppressing the performance degradation of layered NCM811 cathode during high temperature (HT) operation. Through a series of advanced characterization techniques including *in/ex situ* Bragg coherent diffractive imaging (BCDI), *in situ* focused-ion-beam scanning electron microscopy (FIB-SEM) and transmission electron microscopy (TEM), and *in situ* high-energy X-ray diffraction coupled with mass spectrometry (HEXRD-MS), we systematically investigated the structural transformation of NCM811 cathode w/ and w/o PEDOT coating during cycling aging, calendar aging and thermal runaway, and from atomic scale to single primary particle, single secondary particle and bulk powder level. Our results showed that HT and high SoC aging will significantly accelerate the transition metal dissolution and surface reconstruction, mechanical cracking and oxygen outgassing of NCM811 cathodes. Thanks to the HF scavenging effect and mechanic robustness of PEDOT, the aforementioned issues have been effectively mitigated, leading to significantly improved HT operational tolerance. The present findings provide new insights into the failure mechanism of LIBs at

high temperature and will inspire more efforts in the surface structure control of battery materials towards harsh operation.

2. Results and discussion

Our previous study has revealed that PEDOT coating at both primary and secondary particle levels could effectively improve the cycle stability of various layered oxide cathodes towards high-voltage operation.[21] Nevertheless, its effectiveness at high-temperature in particular during HT calendar aging and thermal runaway of Ni-rich cathodes and the fundamental origins remain unclear, which is also true for other surface coating. Herein, we performed PEDOT coating on commercial polycrystalline NCM811 cathode using our previously developed oxidative chemical vapor deposition (oCVD) process (see experimental for details) and revealed its effectiveness towards HT operational resiliency.

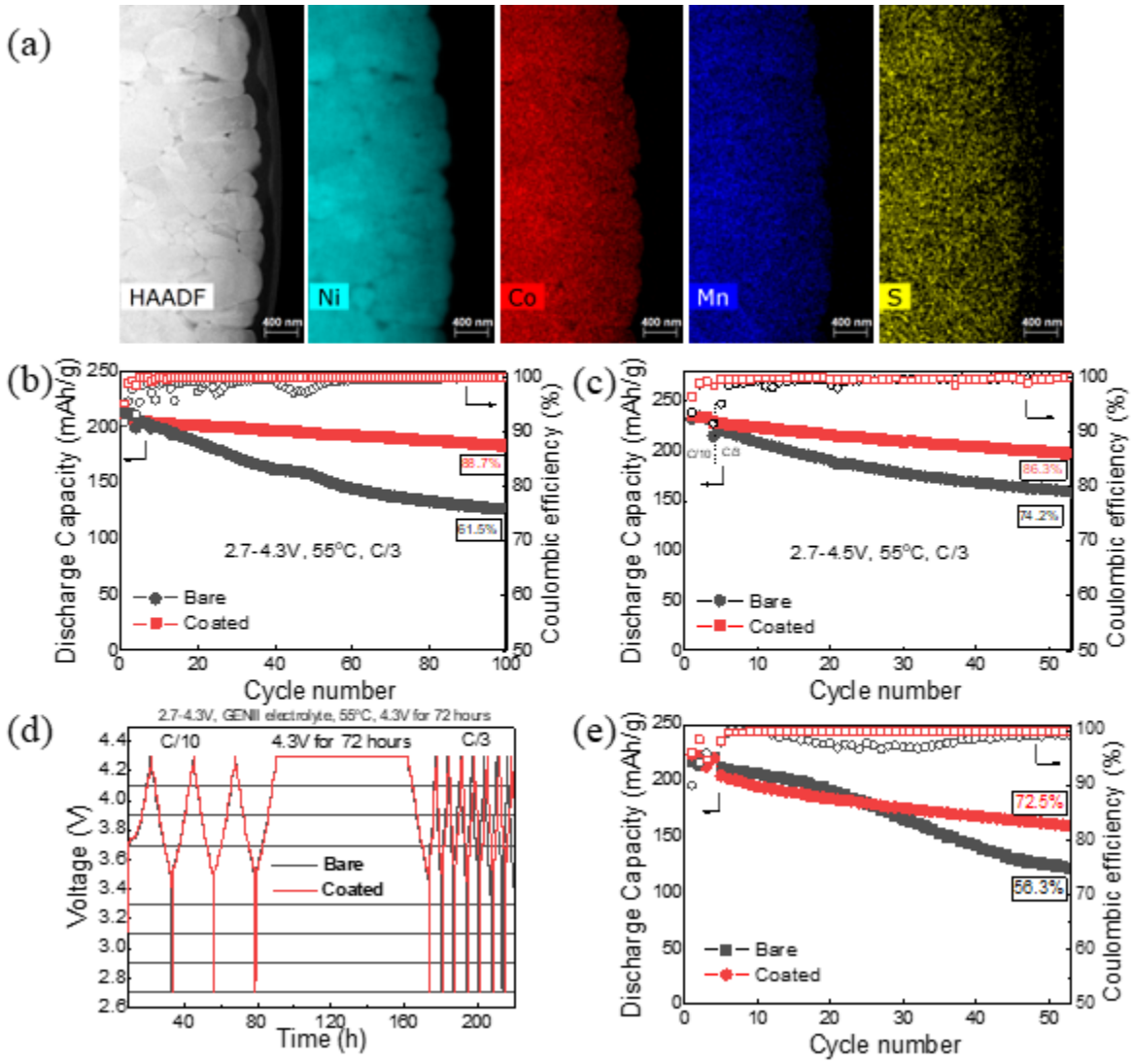

Figure 1. (a) STEM-HAADF-EDS elemental mapping of coated NCM811 particles. Cycling performance of bare and coated NCM811 cathode at C/3 and 55 °C within (b) 2.7-4.3 V and (c) 2.7-4.5 V. (d) Voltage-time curve and (e) corresponding cycling performance of bare and coated NCM811 cathode during high SoC and high-temperature calendar aging.

Figure S1a and S1b show the SEM images of pristine NCM811 particles, which exhibited characteristic features of polycrystalline layered cathodes. After PEDOT coating, no obvious morphological changes can be observed (Figure S1c and S1d). To confirm the homogenous coating of

PEDOT, scanning transmission electron microscopy high-angle annular dark-field energy-dispersive X-ray spectroscopy (STEM-HAADF-EDS) elemental mapping of coated NCM811 cathode was conducted. As shown in **Figure 1a**, in addition to the uniform distribution of Ni, Co and Mn, the signature element of PEDOT—S was homogeneously distributed at both primary and secondary particles of NCM811 cathode. This PEDOT coating layer can thus provide comprehensive protection against the attack of electrolytes especially during HT cycling and calendar aging.

Figure 1b shows the cycling performance of bare and coated NCM811 cathodes during charge/discharge within 2.7-4.3 V (verse Li/Li^+) at 55 ^oC. The cells were under formation at C/10 (1C=200 mA/g) for 3 cycles and then cycled at a higher charge/discharge rate of C/3. The initial columbic efficiency of the coated NCM811 was 95.1% in comparison with 91.6% for bare one, indicating reduced side reactions by the ultra-conformal PEDOT coating. Moreover, the coated NCM811 cathode exhibited a high capacity retention of 88.7% with a high reversible capacity of 182.4 mAh/g after 100 cycles, demonstrating excellent HT cycling stability. By sharp contrast, after 100 cycles, the bare NCM811 cathode can only maintain a low specific capacity of 125.5 mAh/g, corresponding to a low capacity retention of 61.5%. Furthermore, the voltage decay of the NCM811 cathode was also mitigated with the existence of PEDOT coating (Figure S2). The initial average discharge voltage for both bare and coated cathode are about 3.82 V. After 100 cycles, the coated cathode still exhibited an average discharge voltage of 3.76 V, much higher than bare one (3.56 V), indicating much less phase transformation during cycling. When increasing the cut-off voltage to 4.5 V that corresponds to a higher amount (90 mol %) of Li^+ extraction, the 1st charge capacity and columbic efficiency of coated NCM811 cathode were measured to be 243.8 mAh/g and 96.4%, respectively, compared with 248.3 mAh/g and 93.4% for bare one. Meanwhile, the coated cathode presented a much higher capacity (197.3 mAh/g) than bare cathode (159.3 mAh/g) after charge/discharge at C/3 and 55 oC for 50 cycles (Figure 1c), leading to a higher capacity retention of 86.3% than bare NCM811

(74.2%). To evaluate the effectiveness of PEDOT coating in mitigating the calendar aging of NCM811 cathode, both cathodes were under formation for 3 cycles and then charged to 4.3 V and further held at 4.3 V for 72 h at 55 ºC (Figure 1d). After that, the cells were further cycled at C/3 for 50 cycles. In general, the calendar aging resulted in compromised electrochemical performance for both cathodes. The results indicated that calendar aging at high SoC and HT, even for a limited time of period, could cause severe capacity loss, which need to be paid more attention to during practical use of LIBs. Nevertheless, it can be seen that PEDOT coating is able to mitigate such degradation, with a reversible capacity of 159.8 mAh/g and capacity retention of 72.5%, in comparison with only 121.4 mAh/g and 56.3% for bare NCM811 cathode.

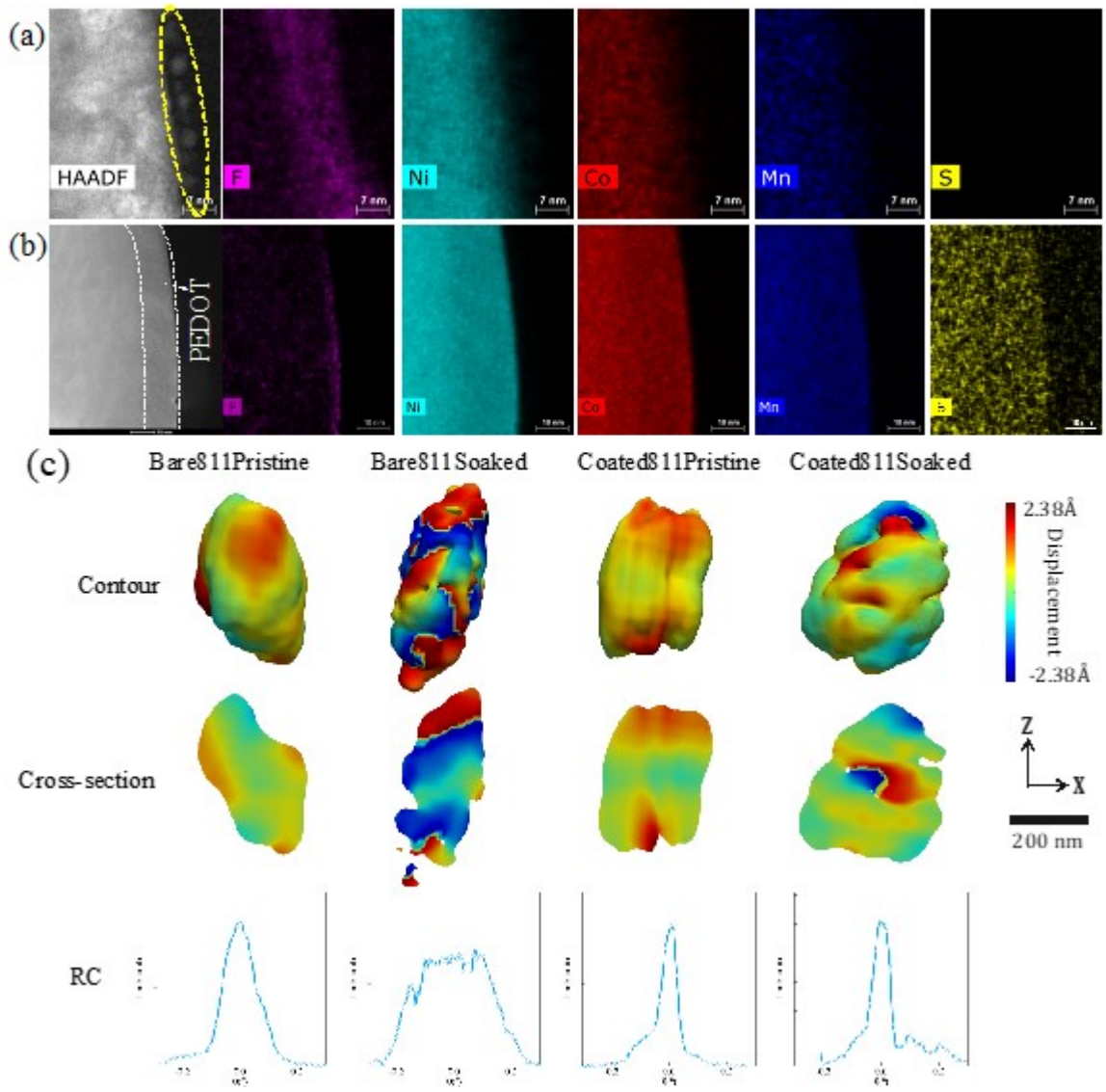

Figure 2. STEM-HAADF elemental mapping of (a) bare and (b) coated NCM811 cathode particle after calendar aging at 4.3 V and 55 ºC for 72 h. (c) Examples of ex-situ BCDI results from typical primary particles of bare NCM811 and coated NCM811 materials before and after aging in electrolyte. The top row shows the contour of the reconstructed particles, the second row shows the cross section at the center along y-axis and the last row shows the rocking curves (RC) of the particles, respectively.

To understand the origin of the electrochemical performance difference between bare and coated cathode during abusive calendar aging, we firstly performed advanced TEM characterization on the aged NCM811 electrodes, which were under formation for 3 cycles and then charged to 4.3 V and held

at 4.3 V for 72 h at 55 °C, followed by discharged to 2.7 V and then disassembled for characterization. **Figure 2a** shows the STEM-HAADF-EDS element mapping of bare NCM811 electrode after HT and high SoC aging. The results showed that electrolytes (represented by the F element) have penetrated into the surface of NCM811 cathode by around ~ 15 nm. Accordingly, the surface of NCM811 cathode became much less densified, indicating a severe surface reconstruction. In addition, the electrolyte (F element) penetration effect was also confirmed with a lower magnification to show several primary NCM particles on the HAADF image and EDX mapping, see Figure S3. More specifically, clear evidence of transition metal dissolution can be seen, as highlighted by the dot-yellow circle in Figure 2a. Such results come from two aspects. On the one hand, it has been reported that the concentration of HF impurity in the electrolytes at HT will be increased, which can thus lead to the loss of cathode active materials.[4] On the other hand, high SoC NCM811 cathode containing Ni^{4+} can further aggravate the parasitic reactions with the electrolytes. Our previous study has revealed that PEDOT can chemically coordinate with HF through formation of O-H-F covalent bonds and hence effectively mitigate the attack of HF towards layered cathodes.[21] To confirm such erode effect of HF, synchrotron X-ray absorption characterization were conducted to detect the valence state and local structure change of the NCM811 cathode after cycling, the results are shown in Figure S4 in the supporting information. Meanwhile, as shown in Figure 2b, the thickness of PEDOT coating layer is around 10 nm, which is mechanically stable during high SoC and high temperature calendar aging. Thus, the PEDOT can act as a shielding layer to prevent the direct contact between electrolytes and NCM811 cathodes, which can stabilize the cathode-electrolytes interface. Therefore, as clearly shown in Figure 2b, F mostly appeared on the outer surface of aged coated NCM811 cathode. Moreover, the surface of coated NCM811 cathode after calendar aging remained smooth, and the PEDOT remained intact, as can be seen from the uniform distribution of Ni, Co, Mn and S.

To directly visualize the structural changes of NCM811 cathode, especially at the primary particle level during calendar aging, we further conducted BCDI characterization. BCDI is a non-destructive X-ray imaging method based on coherent X-rays and phase-retrieval algorithms, which can reconstruct the sample structural, morphological and inner strain information of nanocrystals in three dimensions (3D).[22-24] Recently, it has been used to image the dislocations and microstrain within nanoscale resolution and their dynamics in battery cathode particles during charge/discharge.[25-28]

Figure 2c shows typical examples of primary particles from bare NCM811 and coated NCM811 before and after the aforementioned HT and high SoC aging. 3D diffraction patterns of the [003] reflect were collected from multiple primary particles and reconstructed to show the 3D electron density and phase information. The retrieved the phase information, plotted in colors, reflects the atomic displacement (strain) projected along the [003] reflection. For clarification, since only [003] reflection was measured during the experiment, the displacement and nano-strain are referred to the displacement or strain field projected to the [003] direction. The contour shows the morphology, the cross-section perpendicular to y-axis shows the intraparticle information. The rocking curves (RC) indicate the number of domains and the crystal quality inside the primary particles. The particles from pristine NCM811 have smooth morphology and the displacement fluctuates gradually throughout the entire particle. However, after aging, the bare NCM811 shows strong displacement on both surface and interior of the particle. The intense red and blue color interface indicates a dislocation layer. In addition, the morphology becomes rougher. By sharp contrast, the coated NCM811 accumulated much less strain throughout the particle. Only one dislocation domain was observed near the center of the cross-section, while the rest of the area shows smooth change in atomic displacement. After aging, the rocking curve of the bare NCM811 particle becomes broad without sharp peak that agree with the 3D morphology and the strain projected to [003] direction. Conversely, although the coated NCM811 crystal shows more strain throughout the particle in comparison with the pristine one, the rocking curve has a similar

line shape and width as the pristine particle. In general, the TEM and BCDI results have confirmed that PEDOT can well protect NCM811cathode from electrolytes corrosion, resulting in well-maintained crystallographic structure and hence better battery performance.

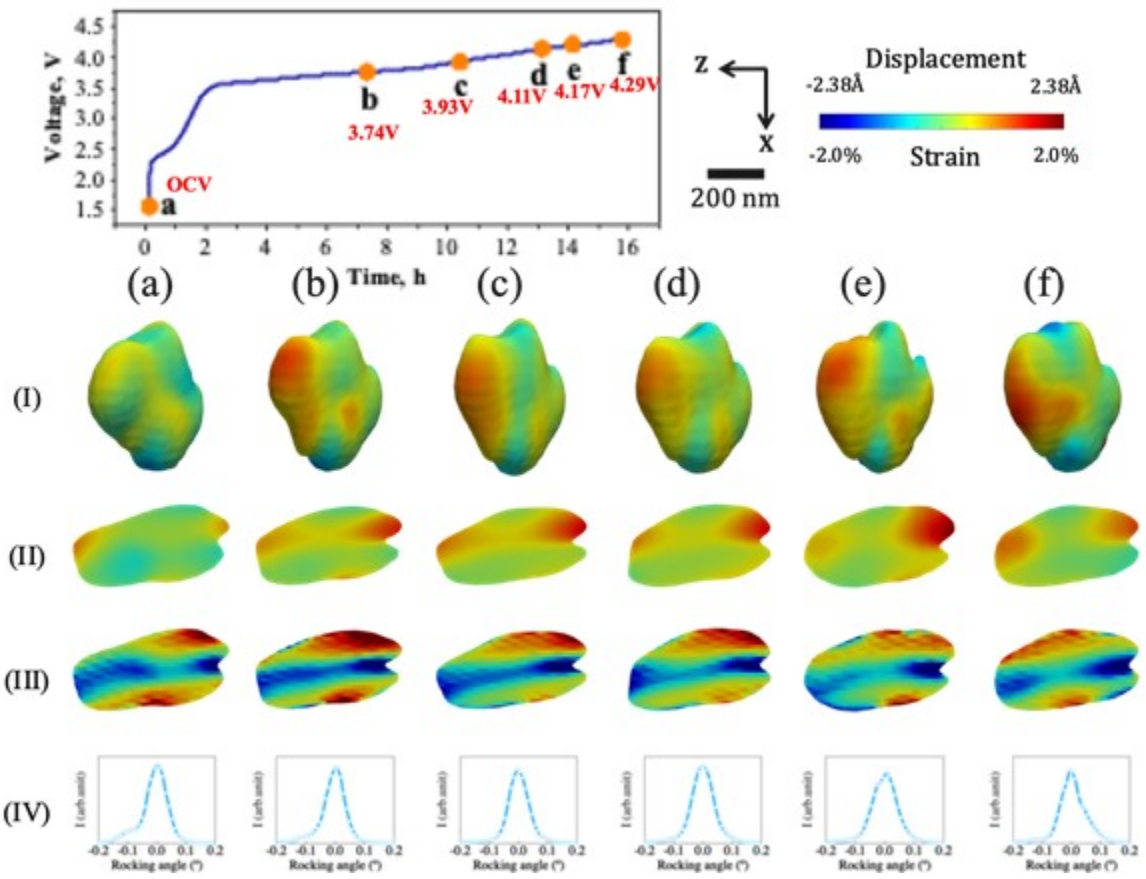

Figure 3. In situ BCDI characterization on coated NCM811 cathode during charge from OCV to 4.3 V. (a-f) corresponds to different voltage points in the charge voltage curve. Row I, II, III, IV represent 3D isosurface rendering, cross-section atomic displacement, strain distribution and rocking curves at different voltage.

One of the advantages of synchrotron X-ray is its capability for *in situ* measurements, which can provide the structural information during charge/discharge of battery materials. Hence, we further conducted *in situ* BCDI on coated NCM811 cathode during charge from open circuit voltage (OCV) to

4.3 V to map the displacement field and dislocation as well as strain distribution inside the primary particles. Noted that the experiment was performed at room temperature, and the weight ratio of active materials in the electrodes for BCDI measurement is 40 wt.% for monodispersed NCM particles to obtain better imaging quality, see Experimental Details. The *in situ* BCDI during high-temperature charge/discharge requires a special heating environment, which is still under development at synchrotron beamline. Nevertheless, we believe that the RT BCDI results presented here will be fruitful for the explanation of HT working mechanism. Recently, Estandarte et al. have performed *in situ* BCDI measurement on bare NCM811 cathode during charge from 2.7 to 4.1 V followed by discharge to 3.9 V, which can serve as a comparison with our coated NCM811 cathode.[26] Their results revealed that non-uniform distributions of inter- and intra-crystal strain existed at all SoC of bare NCM811 particle, leading to crystal domain distortion, splitting and shrinkage, and eventually particle cracking during charge/discharge.

Figure 3 shows the charge voltage curve of coated NCM811 cell with Li as counter electrode and the selected data points (a-f) during *in situ* BCDI measurement. Row (I) shows the 3D isosurface reconstruction images of coated NCM811 particle at different charge voltage, which can reflect the evolution of overall crystal shape during charge. Unlike the bare NCM811 that undergoes substantial crystal volume reduction and crystal splitting when charged from 2.7 V to 3.5 V,[26] the coated NCM811 particle did not show visible particle shape change even when charged to 4.3 V. The results indicated that no breakdown of crystals occurred in the case of coated NCM811 crystal during charge. This conclusion can be further corroborated by their corresponding central Bragg diffraction patterns, which did not show obvious broadening or pixel shift (Figure S5).

Row (II) compares the cross-section displacement field of coated NCM811 particle during extraction of Li^+, which were taken near the center of the crystal imaged with the [003] direction. The positive and negative value means atomic displacement from the ideal crystal lattice along or opposite

to direction of the *q*-vector, *i.e.* [003] direction in this work. Before charge (point a), we can observe a continuous displacement field with only a slight deviation on the surface, which might be due to the existence of minor lattice defects during synthesis. After charging to 3.74 V (point b), the positive displacement on the surface of crystal gradually increased. This may be because of the faster Li^+ de-intercalation kinetic on the surface of battery particles, which can lead to slightly higher SoC on the surface in comparison with inner crystal domains. Further charging the coated NCM811 crystal from 3.74 V to ~ 4.3 V did not trigger dramatic changes on the displacement field. By comparing the displacement field during the charge process, we can conclude that there is no appearance of singularity characteristic of dislocation, which is in contrast to that observed in the bare NCM811[26] or $LiNi_{0.85}Co_{0.1}Al_{0.05}O_2$[25] cathodes during charge. The corresponding strain field distribution of the coated NCM811 crystal during charge was further shown in row (III), which exhibited only slight changes during the whole charge process. The corresponding rocking curves during charge remained one center, indicating no cracking inside the crystal during charge. This is also contradictory to the bare NCM811 crystal during charge, which exhibited peak splitting after charge.[26] Therefore, the *in situ* BCDI results have confirmed that the PEDOT coating can effectively prevent the structural degradation (e.g. intragranular cracking) of NCM811 cathode within the primary particles level.

For conventional polycrystalline layered cathodes, the primary nanoparticles were further assembled into micrometer-sized secondary particles to increase the packing density. However, the secondary particles tend to suffer from intergranular cracking and the associated electronic isolation of active materials as well as side reactions with the electrolytes. Therefore, intergranular cracking has been considered as another major degradation origin during cycling of layered cathodes. To reveal the structural changes at the secondary particles level, we further conducted *in situ* FIB-SEM characterization on both bare and coated NCM811 cathode during charge/discharge. **Figure 4a** shows the schematic image of our set up, which can monitor the morphology changes of single battery particle

during charge/discharge. In our previous works, we have used this setup to reveal the volume changes of many alloying-based anodes during (de) lithiation.[29-33] Here we further used it to understand how PEDOT coating help mitigate the intergranular cracking of NCM811 cathode during charge/discharge.

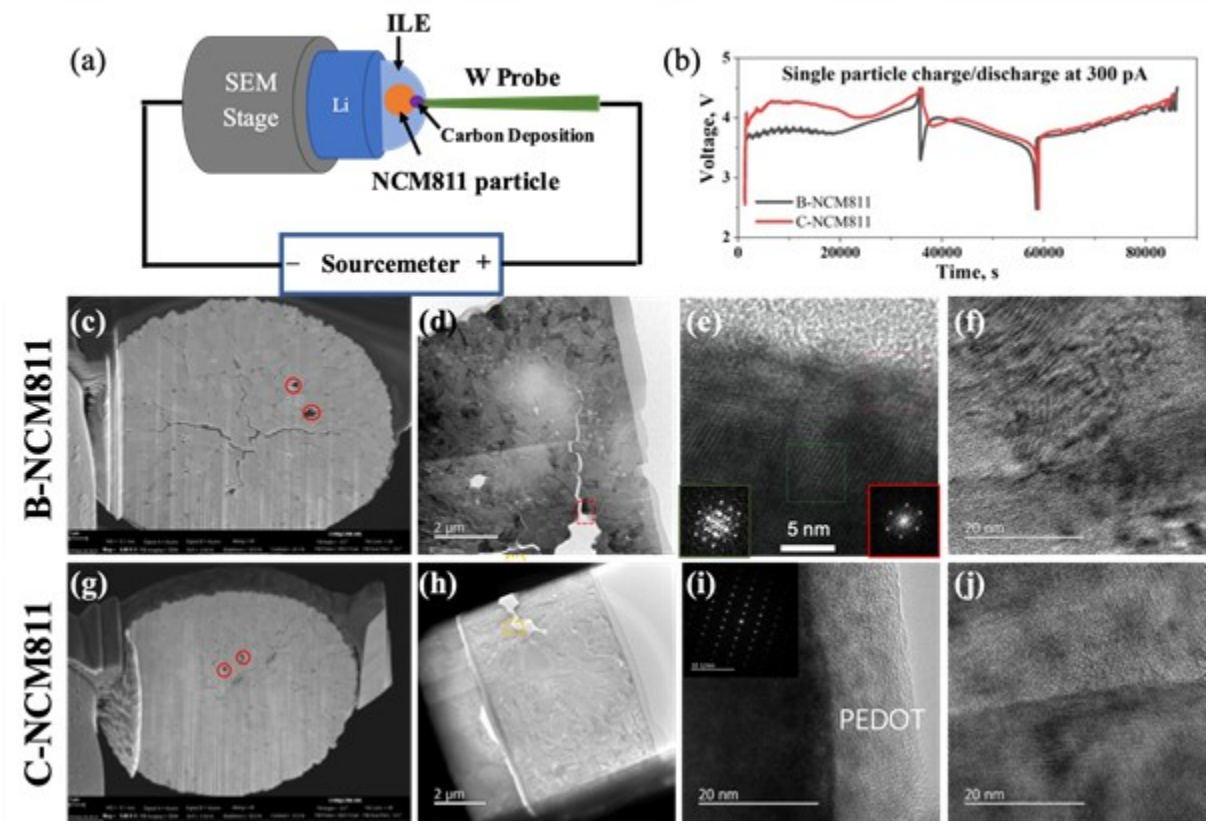

Figure 4. (a) In situ FIB-SEM set up and (b) corresponding charge/discharge curves of single bare and coated NCM811 secondary particle. (c) cross-section SEM image and the corresponding (d-f) TEM images of bare NCM811 particle after charge/discharge test in (b). (g) cross-section SEM image and the corresponding (h-j) TEM images of coated NCM811 particle after charge/discharge test in (b). Inset in (i) is the selected area diffraction pattern to show the layered structure. The red circles in (c) and (g) indicates the native pores inside NCM811 particles that was induced during synthesis. The rectangle in (d) and (h) represents the particle characterized in (e-f) and (i-j), respectively.

Figure 4b shows the voltage-profiles of single bare and coated NCM811 particle during charge/discharge at 300 pA (~ C/10) within 2.7-4.5 V, similar to that in the coin-cell. The particles were charged to 4.5 V and then taken out for advanced FIB-SEM and TEM characterization. Figure 4c shows the cross-section SEM image of bare NCM811 cathode after the aforementioned charge/discharge test. Noted that the nanometer-sized voids marked by red circles were induced during the coprecipitation synthesis of NCM811 precursors and calcination of cathodes due to the release of CO_2 or H_2O vapor during the calcination (Figure S6). After cycling, the bare NCM811 particle exhibited severe intergranular cracking along grain boundaries, which is not surprising and has been *in*/*ex* situ observed in NCM811 cathodes when they are charged to high voltage.[34-36] It is believed that the anisotropic changes in lattice parameter of different grains during extraction/insertion of Li^+ are the major cause for such intergranular cracking.[37] Figure 4d shows the cross-section TEM image of the cycled bare NCM811 slice. We have measured high resolution TEM on the particle (marked by red rectangle) nearby the cracking region. As shown in Figure 4e, the outer surface of the particle exhibited severe surface reconstruction with formation of rock-salt phase structure in the thickness about 10-20 nm. In the inner particle, we can observe clear curvature in the lattice fringes (Figure 4f), indicating the existence of huge stress at the nanoscale after high-voltage charge. In the case of PEDOT-coated NCM811 cathode, we observed a significantly different result. As shown in Figure 4g and 4h, the 4.5V-charged coated NCM811 particle did not exhibit severe intergranular cracking, indicating that the ultraconformal PEDOT at both primary and secondary particle level could effectively mitigate the intergranular cracking. This might be because PEDOT could serve as a soft buffer layer to accommodate the mechanical stress at the grain boundaries. As shown in Figure 4i, the PEDOT coating layer remained well preserved after high-voltage charge, indicating good mechanical robustness. Therefore, coated NCM811 cathode did not undergo surface reconstruction and can well maintain its layered structure, as shown in the selected area diffraction pattern in Figure 4i and Figure 4j.

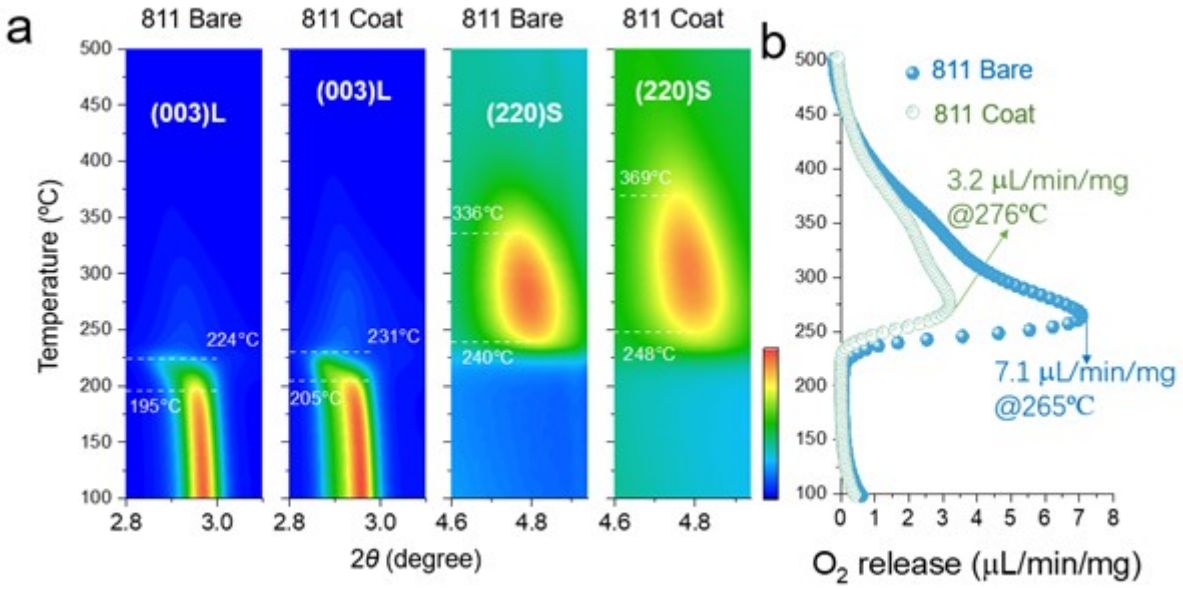

Figure 5. *in situ* phase transformation and oxygen outgassing of the charged bare NCM811cathode and with coating during heating. (a)The contour plots of the layered $(003)_L$ diffraction peak fading and spinel $(220)_S$ peak emerging. (b) The comparison of oxygen outgassing behavior of the 4.5V-charged bare and coated NCM811 cathodes during heating.

The *in situ* BCDI and FIB-SEM results on single primary and secondary particle have collectively revealed that PEDOT coating can alleviate the mechanical stress inside and between the primary particles. Nevertheless, characterization (e.g. XRD) on millions of particles should be conducted to provide the structural transformation at bulky level. Hence, we further performed *in situ* high-energy XRD (HEXRD) coupled with mass spectrometry to reveal the effect of PEDOT coating on the structural transformation and oxygen outgassing of delithiated NCM811 cathode during high temperature heating, which are highly related to the thermal tolerance and safety performance of layered cathodes. **Figure 5a** compares the 2D contour plot of layered $(003)_L$ and spinel $(220)_S$ peaks during heating of 4.5V-charged NCM811 cathodes from room temperature to 500 °C, with red and blue color represent high and low intensity, respectively. Upon heating, the transition metal cations of layered structure migrated through the face-sharing tetrahedra site to the neighboring lithium vacancy octahedra site, leading to a

layered-to-spinel structural transformation.[12] The $(003)_L$ peak of 4.5V-charged bare NCM811 cathode started to fade at a temperature of 195 ºC and completely disappeared at 224 ºC. Accordingly, we can observe the emerging of $(220)_S$ peak at a temperature of ~240 ºC in the case of delithiated bared NCM811 cathode. Upon further heating, the spinel phase was converted to rock salt phase starting at 339 ºC. These results can be seen more clearly in the waterfall HEXRD patterns and the peaks assignment shown in Figure S5. By contrast, we found PEDOT coating has postponed the structural transformation of layered-spinel-rock salt to higher temperature of 205 ºC, 231 ºC, 248 ºC and 369 ºC, respectively (Figure 5a & Figure S7).

In addition to the phase transformation, we simultaneously monitored the oxygen outgassing of 4.5V-charged NCM811 cathodes during heating, which can trigger the breakdown of layered structures.[38-41] As shown in Figure 5b and Figure S8, the oxygen outgassing of delithiated bare NCM811 cathode started from ~220 ºC, which is consistent with critical temperature of the aforementioned phase transformation process, and then abruptly increased to the maximum O_2 release rate of 7.1 μL/min/mg at 265 ºC. Strikingly, the coated NCM811 cathode suppressed the oxygen release with a rate of only 3.2 μL/min/mg and at a higher temperature of 276ºC. In other words, the heat generation of delithiated coated NCM811 cathode associated with the oxygen gas can be reduced by 50% compared with the bare one. These results suggest that PEDOT coating can significantly improve the thermal stability of layered NCM811 cathodes at the bulk level, which can thus prompt its safety performance and high temperature operational resiliency.

3. Conclusion

High temperature operational resiliency especially calendar aging and thermal runaway of lithium-ion batteries are essential for their practical use under extreme environment. In this work, the multi *in/ex-situ* electron microscopy and synchrotron X-ray imaging/diffraction techniques enabled a systematic understanding on the surface structure effects of layered oxide cathodes in tailoring their

high temperature behavior. Our results showed that when exposed to high temperature, high state-of-charge layered cathodes undergo accelerated phase transformation, mechanical cracking and oxygen release throughout different length of scale. Furthermore, we revealed that an ultraconformal PEDOT coating could effectively tackle these issues, significantly improving the operational tolerance of commercial NCM811 cathode under high SoC and high temperature situations. The present work has shed new light on the high temperature degradation mechanism of Ni-rich cathodes and established a design rule for rational surface protection towards harsh operation.

4. Experimental

Bare and PEDOT-coated NCM811 cathodes: Bare NCM811 was purchased from MTI Corp. Poly(3,4-ethylenedioxythiophene) (PEDOT) coating was conducted on the NMC811 particles using an established rotary oCVD system described in our previous work.[21] 3,4-Ethylenedioxythiophene (EDOT) monomer (Clevios™ M V2, Heraeus, 98.5% purity) and $VOCl_3$ (Sigma-Aldrich, 99% purity) were used as the raw materials for PEDOT coating without purification. To perform the coating, the EDOT and $VOCl_3$ were heated in a temperature-controlled glass jar at the temperature of 140 and 30 °C, respectively. The EDOT and $VOCl_3$ vapors were introduced into the reactor in the flow rate of 2±0.2 and 0.2±0.05 SCCM (SCCM stands for standard cubic centimeter per minute), respectively, along with N_2 carrier gas (5±0.2 SCCM). The reactor pressure was maintained at approximately 300 mTorr by an exhaust valve and the heating bath was kept at 80 °C while the rotation rate was set at 140-160 r.p.m., throughout the whole oCVD process. After 60 minutes of coating, the sample was rinsed a few times with methanol and tetrahydrofuran followed by drying in a vacuum oven for 2 hours to obtain the PEDOT coated NCM811 sample.

Electronic microscopy characterization: *In situ* FIB-SEM during charge/discharge of bare and coated NCM811were conducted on a Zeiss NVision 40 FIB-SEM system.[33, 36] Typically, we used a tungsten probe to get single particle via ion beam carbon deposition. The electrolyte used in the experiments was

ionic liquid based electrolytes consisting of 10 wt.% LiTFSI in 90 wt.% P_{14}TFSI. Li metal was used as reference electrode and attached on a SEM stage. The cell was charged/discharged using a Keithley 6430 Sub-Femtoamp Remote SourceMeter® from Tektronix within 2.7-4.5 V at 300 pA. The morphology and structures of bare and coated NCM811 were further characterized by transmission electron microscopy (FEI Talos F200X TEM/STEM), in which the TEM samples were prepared through standard lift-out procedure.

BCDI measurement: The Bragg Coherent X-ray Diffractive Imaging experiment was performed at the 34-ID-C beamline of the Advanced Photon Source, Argonne National Laboratory. X-rays were selected by a Si (111) double crystal monochromator at 9keV energy and collimated by a pair of beam-defining slits to full coherence. The X-ray beam is then focused onto the sample with ~600 nm in diameter. 3D diffraction patterns were collected by a single photon counting Timepix detector with oversampling at a frequency finer than the Nyquist interval. The 3D diffraction patterns were recorded repeatedly during the *in situ* experiment while the coin cell is charged from OCV to 4.3V without holding the voltage. The detailed experimental setup and data collection protocols can be found in our previous work.[22] A low active materials loading with the active material (NCM811):conductive carbon:binder of 4:4:2 rather than 8:1:1 was used, aiming to obtain monodispersed NCM811 particles for better imaging quality. As revealed by Manthiram et al.,[42] the conductive carbon could influence the cathode-electrolyte interfaces that was initially formed on conductive carbon even with no electrochemical bias applied, which can readily passivate the cathode particles through mutual exchange of surface species. As a result, the increased conductive carbon led to a small plateau at ~ 2.5 V. The rocking curves plot the integrated intensity of 2D diffraction patterns as a function of the sample rocking angle near its Bragg condition. The 3D diffraction patterns were reconstructed using a linear combination of Error Reduction and Hybrid Input-Output algorithms.[43] Shrink-wrap is also used to update the support during the iterative phasing loops.[44-46] The 3D rendering, cross-sections were plotted with Paraview.

Electrochemical test: The bare and coated NCM811 laminates were prepared by mixing the active materials with carbon black and poly(vinyldifluoride) at the ratio of 90:05:05 in N-Methyl-2-pyrrolidone. Then the slurry was coated onto Al foil and dried at 75 ºC overnight. The loading of the active materials is controlled to be ~5 mg/cm^2. Then the 2032 type coin cell was assembled in the glove box with lithium metal as reference/counter electrode and 1M $LiPF_6$ in EC(ethylene carbonate):EMC(ethyl methyl carbonate) (3:7 by volume) as electrolyte. The coin cell test was performed by a MACCOR battery test system at 55 ºC and various charge/discharge conditions. All the cells were under formation at C/10 and then charged/discharged at a higher rate of C/3.

***In situ* HEXRD during heating with mass spectrometry**: The beamline 17-BM of Advanced Photon Source (APS) of Argonne National Laboratory was utilized for the characterization of *in situ* HEXRD with mass spectrometry. The X-ray wavelength was 0.24105Å. At first, the charged powder was collected by disassembling the 4.5V charged coin-cell battery at glove-box, then around 2 mg cathode powder was loaded into the quartz capillary tube system, with controllable heating unit and inner carrier gas flow. A 5 ml/min ultrahigh-purity helium was used as the carrier gas, and a Pfeiffer Vacuum PrismaPlus® QMG 220 residual gas analyzer was used to analyze the cathode outgassing during heating. The heating rate was 5°C/min to 500°C, and each diffraction data was acquired at the rate of 30 seconds/image by a PerkinElmer amorphous silicon 2D detector. Then the 2D image were converted to 1D patterns and analyzed with the GSAS II software.

Supporting Information

Supporting Information is available from the Wiley Online Library or from the author.

Acknowledgements

Xiang Liu, Xinwei Zhou and Qiang Liu contributed to this work equally. Research at Argonne National Laboratory was funded by the US Department of Energy (DOE) Vehicle Technologies Office. Use of

the Advanced Photon Source and Center for Nanoscale Materials, Office of Science User Facility operated for the U.S. Department of Energy (DOE) Office of Science by Argonne National Laboratory, was supported by the U.S. DOE under Contract No. DE-AC02-06CH11357. X.L., G.X., and K.A. acknowledge the support of the U.S. China Clean Energy Research Center (CERC-CVC2). Q.L. and G.C. thank the funding support from Hong Kong Research Grants Council (GRF 15221719), Otto Poon Charitable Foundation (No. 847W) and The Hong Kong Polytechnic University (P0034050).

Received: ((will be filled in by the editorial staff))

Revised: ((will be filled in by the editorial staff))

Published online: ((will be filled in by the editorial staff))

Conflict of Interest

The authors declare no conflict of interest.

Reference

[1] M.-T. F. Rodrigues, G. Babu, H. Gullapalli, K. Kalaga, F. N. Sayed, K. Kato, J. Joyner, P. M. Ajayan, *Nat. Energy* **2017**, 2, 17108.

[2] G.-L. Xu, X. Liu, A. Daali, R. Amine, Z. Chen, K. Amine, *Adv. Funct. Mater.* **2020**, 30, 2004748.

[3] J. D. Steiner, L. Mu, J. Walsh, M. M. Rahman, B. Zydlewski, F. M. Michel, H. L. Xin, D. Nordlund, F. Lin, *Acs Appl. Mater. Interfaces* **2018**, 10, 23842.

[4] S. F. Lux, I. T. Lucas, E. Pollak, S. Passerini, M. Winter, R. Kostecki, *Electrochem. Commun.* **2012**, 14, 47.

[5] H. Gao, J. Cai, G.-L. Xu, L. Li, Y. Ren, X. Meng, K. Amine, Z. Chen, *Chem. Mater.* **2019**, 31, 2723.

[6] M. Dubarry, N. Qin, P. Brooker, *Curr. Opin. Electrochem*. **2018**, 9, 106.

[7] M. Ecker, N. Nieto, S. Käbitz, J. Schmalstieg, H. Blanke, A. Warnecke, D. U. Sauer, *J. Power Sources* **2014**, 248, 839.

[8] H.-H. Ryu, G.-T. Park, C. S. Yoon, Y.-K. Sun, *Small* **2018**, 14, 1803179.

[9] D. Hu, Q. Zhang, J. Tian, L. Chen, N. Li, Y. Su, L. Bao, Y. Lu, D. Cao, K. Yan, S. Chen, F. Wu, *Acs Appl. Mater. Interfaces* **2021**, 13, 6286.

[10] W. M. Seong, K.-Y. Park, M. H. Lee, S. Moon, K. Oh, H. Park, S. Lee, K. Kang, *Energy Environ. Sci.* **2018**, 11, 970.

[11] X. Feng, M. Ouyang, X. Liu, L. Lu, Y. Xia, X. He, *Energy Storage Mater.* **2018**, 10, 246.

[12] X. Liu, G.-L. Xu, L. Yin, I. Hwang, Y. Li, L. Lu, W. Xu, X. Zhang, Y. Chen, Y. Ren, C.-J. Sun, Z. Chen, M. Ouyang, K. Amine, *J. Am. Chem. Soc.* **2020**, 142, 19745.

[13] X. Liu, D. Ren, H. Hsu, X. Feng, G.-L. Xu, M. Zhuang, H. Gao, L. Lu, X. Han, Z. Chu, J. Li, X. He, K. Amine, M. Ouyang, *Joule* **2018**, 2, 2047.

[14] X. Liu, L. Yin, D. Ren, L. Wang, Y. Ren, W. Xu, S. Lapidus, H. Wang, X. He, Z. Chen, G.-L. Xu, M. Ouyang, K. Amine, *Nat. Commun.* **2021**, 12, 4235.

[15] S. Kalluri, M. Yoon, M. Jo, S. Park, S. Myeong, J. Kim, S. X. Dou, Z. Guo, J. Cho, *Adv. Energy Mater.* **2017**, 7, 1601507.

[16] H. Yang, H.-H. Wu, M. Ge, L. Li, Y. Yuan, Q. Yao, J. Chen, L. Xia, J. Zheng, Z. Chen, J. Duan, K. Kisslinger, X. C. Zeng, W.-K. Lee, Q. Zhang, J. Lu, *Adv. Funct. Mater.* **2019**, 29, 1808825.

[17] P. Yan, J. Zheng, J. Liu, B. Wang, X. Cheng, Y. Zhang, X. Sun, C. Wang, J.-G. Zhang, *Nat. Energy* **2018**, 3, 600.

[18] J. Kim, H. Ma, H. Cha, H. Lee, J. Sung, M. Seo, P. Oh, M. Park, J. Cho, *Energy Environ. Sci.* **2018**, 11, 1449.

[19] S. E. Jerng, B. Chang, H. Shin, H. Kim, T. Lee, K. Char, J. W. Choi, *Acs Appl. Mater. Interfaces* **2020**, 12, 10597.

[20] C. W. Park, J.-H. Lee, J. K. Seo, W. Y. Jo, D. Whang, S. M. Hwang, Y.-J. Kim, *Nat. Commun.* **2021**, 12, 2145.

[21] G.-L. Xu, Q. Liu, K. K. S. Lau, Y. Liu, X. Liu, H. Gao, X. Zhou, M. Zhuang, Y. Ren, J. Li, M. Shao, M. Ouyang, F. Pan, Z. Chen, K. Amine, G. Chen, *Nat. Energy* **2019**, 4, 484.

[22] L. Li, Y. Xie, E. Maxey, R. Harder, *J. Synchrotron Radiat.* **2019**, 26, 220.

[23] I. Robinson, R. Harder, *Nat. Mater.* **2009**, 8, 291.

[24] I. K. Robinson, I. A. Vartanyants, G. J. Williams, M. A. Pfeifer, J. A. Pitney, *Phys. Rev. Lett.* **2001**, 87, 195505.

[25] A. Singer, M. Zhang, S. Hy, D. Cela, C. Fang, T. A. Wynn, B. Qiu, Y. Xia, Z. Liu, A. Ulvestad, N. Hua, J. Wingert, H. Liu, M. Sprung, A. V. Zozulya, E. Maxey, R. Harder, Y. S. Meng, O. G. Shpyrko, *Nat. Energy* **2018**, 3, 641.

[26] A. K. C. Estandarte, J. Diao, A. V. Llewellyn, A. Jnawali, T. M. M. Heenan, S. R. Daemi, J. J. Bailey, S. Cipiccia, D. Batey, X. Shi, C. Rau, D. J. L. Brett, R. Jervis, I. K. Robinson, P. R. Shearing, *Acs Nano* **2021**, 15, 1321.

[27] T. A. Assefa, A. F. Suzana, L. Wu, R. J. Koch, L. Li, W. Cha, R. J. Harder, E. S. Bozin, F. Wang, I. K. Robinson, *Acs Appl. Energy Mater.* **2021**, 4, 111.

[28] A. Ulvestad, A. Singer, J. Clark, H. Cho, J. W. Kim, R. Harder, J. Maser, Y. Meng, O. Shpyrko, *Science* **2015**, 348, 1344.

[29] X. Liu, B. Xiao, A. Daali, X. Zhou, Z. Yu, X. Li, Y. Liu, L. Yin, Z. Yang, C. Zhao, L. Zhu, Y. Ren, L. Cheng, S. Ahmed, Z. Chen, X. Li, G.-L. Xu, K. Amine, *Acs Energy Lett.* **2021**, 6, 547.

[30] B.-Q. Xiong, X. Zhou, G.-L. Xu, X. Liu, Y. Hu, Y. Liu, L. Zhu, C.-G. Shi, Y.-H. Hong, S.-C. Wan, C.-J. Sun, S. Chen, L. Huang, S.-G. Sun, K. Amine, F.-S. Ke, *Acs Energy Lett.* **2020**, 5, 3490.

[31] R. Amine, A. Daali, X. Zhou, X. Liu, Y. Liu, Y. Ren, X. Zhang, L. Zhu, S. Al-Hallaj, Z. Chen, G.-L. Xu, K. Amine, *Nano Energy* **2020**, 74, 104849.

[32] B.-Q. Xiong, X. Zhou, G.-L. Xu, Y. Liu, L. Zhu, Y. Hu, S.-Y. Shen, Y.-H. Hong, S.-C. Wan, X.-C. Liu, X. Liu, S. Chen, L. Huang, S.-G. Sun, K. Amine, F.-S. Ke, *Adv. Energy Mater.* **2020**, 10, 1903186.

[33] X. Zhou, T. Li, Y. Cui, Y. Fu, Y. Liu, L. Zhu, *Acs Appl. Mater. Interfaces* **2019**, 11, 1733.

[34] J.-H. Kim, S. J. Kim, T. Yuk, J. Kim, C. S. Yoon, Y.-K. Sun, *Acs Energy Lett.* **2018**, 3, 3002.

[35] P. Yan, J. Zheng, T. Chen, L. Luo, Y. Jiang, K. Wang, M. Sui, J.-G. Zhang, S. Zhang, C. Wang, *Nat. Commun.* **2018**, 9, 2437.

[36] D. J. Miller, C. Proff, J. G. Wen, D. P. Abraham, J. Bareño, *Adv. Energy Mater.* **2013**, 3, 1098.

[37] H. Liu, M. Wolf, K. Karki, Y.-S. Yu, E. A. Stach, J. Cabana, K. W. Chapman, P. J. Chupas, *Nano Lett.* **2017**, 17, 3452.

[38] L. Mu, R. Lin, R. Xu, L. Han, S. Xia, D. Sokaras, J. D. Steiner, T.-C. Weng, D. Nordlund, M. M. Doeff, Y. Liu, K. Zhao, H. L. Xin, F. Lin, *Nano Lett.* **2018**, 18, 3241.

[39] S. M. Bak, K. W. Nam, W. Chang, X. Q. Yu, E. Y. Hu, S. Hwang, E. A. Stach, K. B. Kim, K. Y Chung and X. Q. Yang, *Chem. Mater.* **2013**, 25, 337.

[40] E. Y. Hu, S. M. Bak, J. Liu, X. Q. Yu, Y. N. Zhou, S. N. Ehrlich, X. Q. Yang and K. W. Nam, *Chem. Mater.*, **2014**, 26, 1108.

[41] E. Y. Hu, S. M. Bak, S. D. Senanayake, X. Q. Yang, K. W. Nam, L. L. Zhang, M. H. Shao, *J. Power Sources*, **2015**, 277, 193.

[42] W. Li, A. Dolocan, P. Oh, H. Celio, S. Park, J. Cho and A. Manthiram, *Nat. Comm.*, **2017**, 8,

14589.

[43] J. R. Fienup, *Appl. Opt.* **1982**, 21, 2758.

[44] R. P. Millane, W. J. Stroud, *J. Opt. Soc. Am. A* **1997**, 14, 568.

[45] J. N. Clark, X. Huang, R. Harder, I. K. Robinson, *Nat. Commun.* **2012**, 3, 993.

[46] J. N. Clark, J. Ihli, A. S. Schenk, Y.-Y. Kim, A. N. Kulak, J. M. Campbell, G. Nisbet, F. C. Meldrum, I. K. Robinson, *Nat. Mater.* **2015**, 14, 780.

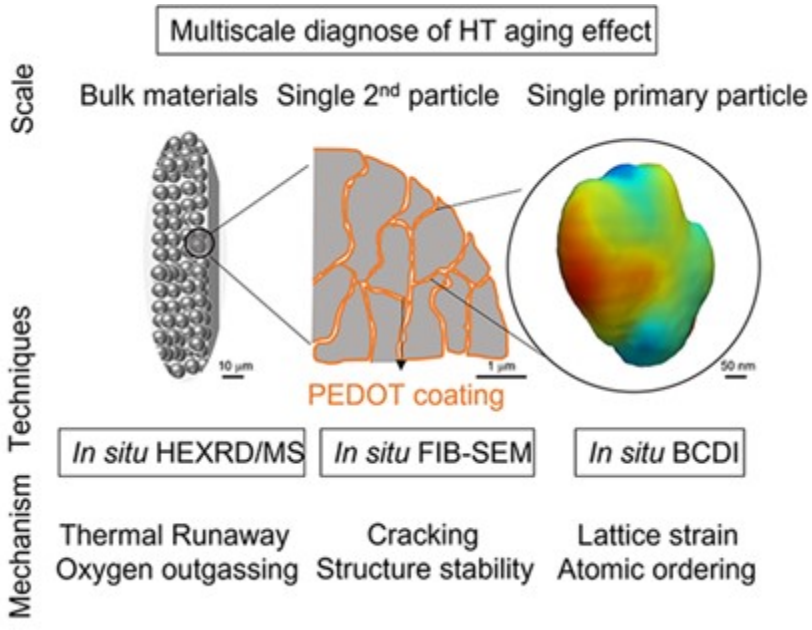

ToC figure

ToC text: High temperature calendar aging and thermal runaway have posted severe performance decay and safety concern on battery cathodes. By using a combination of various in situ synchrotron X-ray and electron microscopy techniques, we report a multiscale understanding of surface structure effects in regulating the high temperature operational resilience of polycrystalline Ni-rich layered cathodes.